Article

A Cross-Scale Analysis of the Correlation between Daytime Air Temperature and Heterogeneous Urban Spaces

Sihong Du [1,2]**, Yanxia Li** [3,4]**, Chao Wang** [3,4]**, Zhichao Tian** [1,2] **, Yongdong Lu** [3,4]**, Sijie Zhu** [3,4] **and Xing Shi** [1,2,]*

1   College of Architecture and Urban Planning, Tongji University, Shanghai 200092, China;
    sihong.du@foxmail.com
2   Key Laboratory of Ecology and Energy-Saving Study of Dense Habitat (Tongji University),
    Ministry of Education, Shanghai 200092, China
3   School of Architecture, Southeast University, Nanjing 210096, China; liyanxia@seu.edu.cn (Y.L.);
    230189011@seu.edu.cn (C.W.); zhichao.tian@foxmail.com (Z.T.); ydlu@seu.edu.cn (Y.L.);
    zhusijie@seu.edu.cn (S.Z.)
4   Key Laboratory of Urban and Architectural Heritage Conservation, Ministry of Education,
    Nanjing 210096, China
*   Correspondence: 20101@tongji.edu.cn; Tel.: +86-159-0519-1490

check for
updates

Abstract: The problem of the urban thermal environment is becoming increasingly noticeable in the process of modern urban development. The temperature patterns in central business districts can be more complicated due to the heterogeneous urban spaces and diverse building forms, which need more cross-scale research. This study investigated the correlation between air temperature and urban morphology in a heterogeneous urban district in northeastern China. The thermal environment of the studied district in the summertime was simulated by ENVI-met. A total of 12 morphological indicators were selected to describe the geometric features of the studied district. Curve estimation was employed to quantify the correlation between air temperature and morphological indicators. The results indicate different effects of the morphological indicators of the air temperature on different scales. On a mesoscale, the compactness (Com), building footprint ratio (BFR), enclosure degree (ED) and total height to total floor area ratio (HA) had a significant correlation with the air temperature. On a microscale, only the BFR and ED had relatively steady correlations with the air temperature. The correlation between air temperature and morphological indicators could be influenced by the heterogeneity of the urban morphology, including the diversity of the heights and footprints of buildings and the irregularity of building horizontal arrangement.

Keywords: spatial temperature variation; cross-scale analysis; urban morphological indicators; heterogeneous urban space

1. Introduction

With the population increase and economic development, the urbanization level of the world has been rising. According to a prediction by the UN, 68% of the world's population will live in cities by 2050 [1]. Although cities provide people with many benefits and opportunities, they face serious problems that need to be addressed. One of them is the urban heat island (UHI) effect and the associated deterioration of the urban thermal environment.

A UHI refers to the phenomenon where the temperature in urban areas is higher than that in rural areas [2]. UHIs may deteriorate the outdoor thermal environment, decrease people's thermal comfort

level and even impact regional atmospheric pollution [3,4]. The increase in the indoor cooling load caused by UHIs leads to more consumption of energy and other resources [5]. Hot weather exacerbated by a UHI can result in heat-related illnesses and even death [6].

The intensity of a UHI and its temporal–spatial variations are affected by many factors, among which urban morphology is an important one. Urban morphology is constituted by building dimensions and spacing, the characteristics of artificial surfaces and the amount of green space [7]. Urban morphology affects UHIs in multiple ways. Surfaces of buildings and pavements in urban areas absorb more solar radiation during the daytime. Clustered buildings can reduce the overall wind velocity and trap more longwave radiation due to their geometric and thermal properties. An increase in impervious pavements reduces evaporation and heat dissipation [8].

UHIs are a multiscale phenomenon [9]. Cities incorporate a range of scales at which many of the environmental dynamics are constituted [10]. The study of UHIs and the thermal environment should take into account the influence of climate zones, building forms and parameters affecting shadows and daylight distribution [11]. The study of urban climates can be classified into different scales. Moudon suggested that the scale of urban morphology can be classified into city/region, street/block and building/plot [12]. In this study, we defined them as the macroscale, mesoscale and microscale, respectively.

The research on UHIs on the macroscale focuses on the effect of land use and geographical features on the spatial distribution of air temperature. The land use features include the fraction of built-up areas, impervious surface areas, vegetation areas and water areas [13–16]. The concept of local climate zones (LCZs) was proposed to classify urban areas into several types of region according to their built forms and thermal performance. Surface cover, structures and materials are uniform within the same LCZ [17]. Methods such as cluster analysis are used to divide the city region into several urban climate zones (UCZs). Thermal variables within the same UCZ are relatively homogeneous compared with those in other types of UCZ in cities [18–20].

On the mesoscale, the relationship between urban form and UHIs is a key research subject. Compared with the macroscale, more three-dimensional urban geometric parameters are incorporated and analyzed. In addition, the turbulent flow and the distribution of air temperature and solar radiation can be determined more precisely by field measurements and numerical simulation. The building footprint area, mean building height, total height to total floor area ratio and sky view factor are frequently reported to influence UHIs or air temperature [21–26]. In addition, the complete aspect ratio, frontal area density and mean building volume are found to influence the solar access or wind field [27–30].

On the microscale, the differentiation of physical spaces and forms creates pockets of urban microclimates in cities [8]. Every built element induces its own microclimate around it so that temperature varies in outdoor spaces, even at short distances [31]. It has been observed that high-rise buildings induce various surrounding microclimates due to the effect of shadow projections [32]. Temperatures on the leeward side of buildings are generally lower than those on the windward side because of shading and small advective effects [33].

As discussed above, urban morphology affects UHIs and the urban thermal environment on various scales. As the scale shrinks from the macro- to the microlevel, detailed urban morphological parameters become more influential in determining the UHI intensity and the pattern of the urban thermal environment. Urban morphological parameters and how they affect the urban thermal environment on the macro- and mesoscales have been extensively studied, as evidenced by works such as [13–30]. However, fewer studies are available on the relationship between urban morphology and the urban thermal environment on the microscale [32,33], which may be explained by the following two reasons.

Firstly, the microscale urban morphological features in modern cities are complex, making it difficult to describe them by spatial parameters. Secondly, thermal variations are relatively inconspicuous in evenly distributed building clusters, which were the main concern of previous

research [34–39]. However, thermal variations can be more evident in some modern urban fabrics, such as isolated high-rise building clusters [32]. Although these kinds of urban fabrics have been somewhat studied [22,23], there is still a lack of targeted investigations.

Another research gap in the field is the lack of cross-scale studies of the correlation between urban morphology and the urban thermal environment. Most research works, if not all, focus on one scale, be it the macro-, meso- or microlevel. A common effort is to establish a quantitative relationship between the temperature at measurement points and their surrounding urban morphology on a specific scale. However, the environmental context of cities constitutes a multidimensional issue, so the effects of various factors on different scales should be considered in urban climate studies [11].

The heterogeneous features of urban spaces make the cross-scale approach more necessary. Although it is impossible to find perfectly homogeneous urban spaces in real cities, residential districts and some traditional urban areas spanning hundreds to thousands of meters are fairly homogeneous in that the buildings are evenly distributed and their heights are uniform, both in a relative sense. However, in many modern cities, especially their central business districts, urban spaces exhibit strong heterogeneous features horizontally, vertically and functionally. The spatial distribution of outdoor air temperature in homogeneous urban spaces is relatively uniform, which lowers the thermal contrast on different scales. This phenomenon makes it easier to establish the correlation between the urban thermal environment and urban morphology on a mono scale. Meanwhile, in heterogeneous urban spaces, even the morphological features of adjacent plots can be dramatically different, and outdoor air temperatures exhibit more significant variations. In this situation, the cross-scale approach can be more suitable for investigating the correlation between air temperature and urban morphology.

Considering the background and research gaps discussed above, we have conducted a cross-scale analysis, both theoretically and experimentally, of the thermal environment of the central business district in Shenyang, a major city located in northern China. The studied area represents urban spaces with strong heterogeneity and, therefore, a complex thermal environment. The focus of the research is on determining and understanding the pattern of the thermal environment on different scales and establishing its correlation with the urban form.

The remainder of the paper is organized as follows. Section 2 presents the methodology, including the studied urban district, the model simulation, the scale of analysis and the selection of urban morphological indicators. Section 3 presents the results of the model simulation and curve estimation, including the air temperature patterns on the mesoscale and microscale and their correlations with urban morphological indicators. Section 4 discusses the effect of morphological heterogeneity and scale differences on the correlations. Section 5 concludes the paper.

2. Materials and Methods

2.1. The Urban District Studied

The urban district studied is part of the central business district in Shenyang, a major city in northeastern China with more than 8 million inhabitants. As shown in Figure 1, it is of a rectangular shape with a long side of 1.1 km and a short side of 0.9 km. The district is densely built, with various types of buildings, such as shopping malls, hotels, office buildings, residential buildings, etc.

The local climate is a typical temperate continental monsoon climate [40]. The winter season is long and cold. The monthly average temperature in January is −4.8 °C. The summer season is short and mild. In July, the monthly average temperature is 24.6 °C, and extreme temperatures can exceed 36 °C. The humidity throughout the year is relatively low. The prevailing wind in the summer is 22.5° south-southwest (SSW), and its average speed is 2.8 m/s. The prevailing wind in the winter is 22.5° east-northeast (ENE), and its average speed is 1.9 m/s.

A 3D model of the urban district is shown in Figure 2a. A total of 169 buildings with diversified forms and functions are densely arranged in the district. Typical examples are midrise slab residential

buildings, high-rise tower office buildings and commercial buildings constructed with podiums and towers.

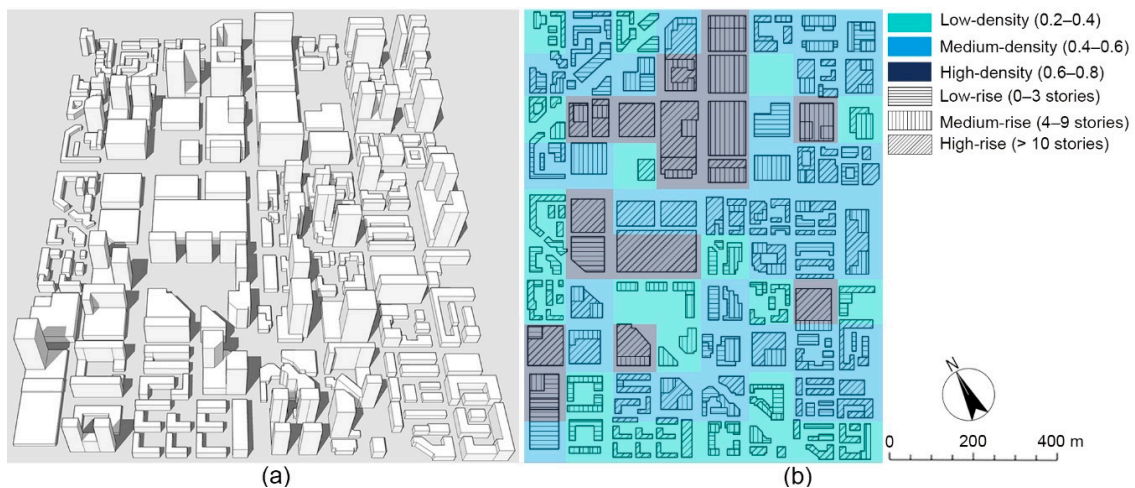**Figure 1.** Location of the studied district and classification of land use functions.

Figure 2. (**a**) A 3D model of the studied district; (**b**) classification of the density of the plot units and heights of buildings.

We calculated the building density and heights of each plot unit with a grid resolution of 100 m and classified these into three grades (Figure 2b). It could be found that the density of the adjacent plots could differ by two grades at most, and the same plot unit contained buildings with different grades of height. The areas of building footprints also ranged from a few hundred square meters to over ten thousand square meters. These geometric features indicate the heterogeneity of the urban morphology of the studied district.

2.2. Scale of Analysis

The investigation of the correlation between air temperature and urban morphology involved the mesoscale and microscale. The mesoscale was defined to be the 3D model domain, i.e., 0.9×1.1 km^2. The spatial dimensions of the microscale were defined as 400×400 m^2. The minimum size of the plot, 400×400 m^2, ensured that the upwind portion could be fully adjusted to its underlying surfaces [17]. Plots smaller than this size are vulnerable to the temperatures of adjacent plots.

For the mesoscale analysis, the morphological indicators were calculated over 200×200 m^2 grids, which were recommended to be a suitable grid size for the study of the relationship between the air temperature and urban morphology in previous studies [22,41]. Their impact on the air temperature of the central representative points of the grids was investigated. For the microscale analysis, this grid size was set to 100×100 m^2, consistent with the typical plot unit in the district (Figure 3).
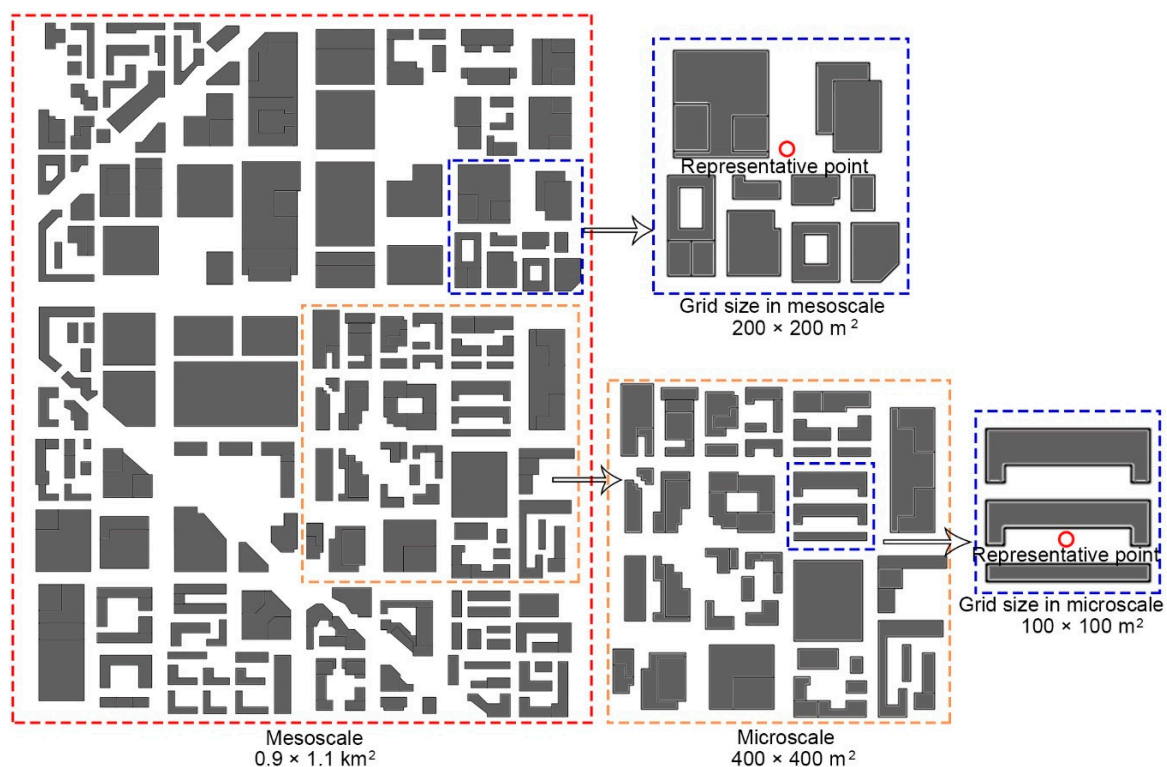

Figure 3. Dimensions for the mesoscale and microscale analysis and their grid sizes.

2.3. Thermal Environment Simulation

The thermal environment of the urban district was simulated in ENVI-met 4.4.3, a holistic 3D nonhydrostatic model for the simulation of surface–plant–air interactions in a complex environment composed of buildings and surfaces with diverse configurations of materials and vegetation [42].

2.3.1. Construction of the Computation Model

The simulation included an experiment scenario and an evaluation scenario. The analyses of this study were based on the simulated results of the experiment scenario, and the evaluation scenario was used to evaluate the reliability of the ENVI-met model. Vegetation was excluded from the two scenarios for two reasons. Firstly, there was little vegetation in the studied district due to its intense development. Moreover, the vegetation factors may affect the statistical correlation between urban morphology and air temperature, especially when they are significantly correlated with some morphological indicators.

In the experiment scenario, the geometric model of the studied district (Figure 1) was fitted to a 180×220 grid system on the horizontal plane, with a resolution of 5 m for each grid. In the vertical

direction, the model contained 30 grids. The resolution of the first 10 vertical grids was 3 m. The lowest grid was further split into five subcells. From the 11th grid upwards, the vertical resolution increased with a telescoping factor of 13% (Figure 4a). In addition, 10 nesting grids were added around the model to improve simulation accuracy (Figure 4b). To align the geometric model with the true direction of the urban district, it was rotated 28° eastward from the north direction. The exterior materials of the buildings in the model were set to be lightweight concrete. The underlying surfaces of the streets and public spaces were defined as concrete pavement.
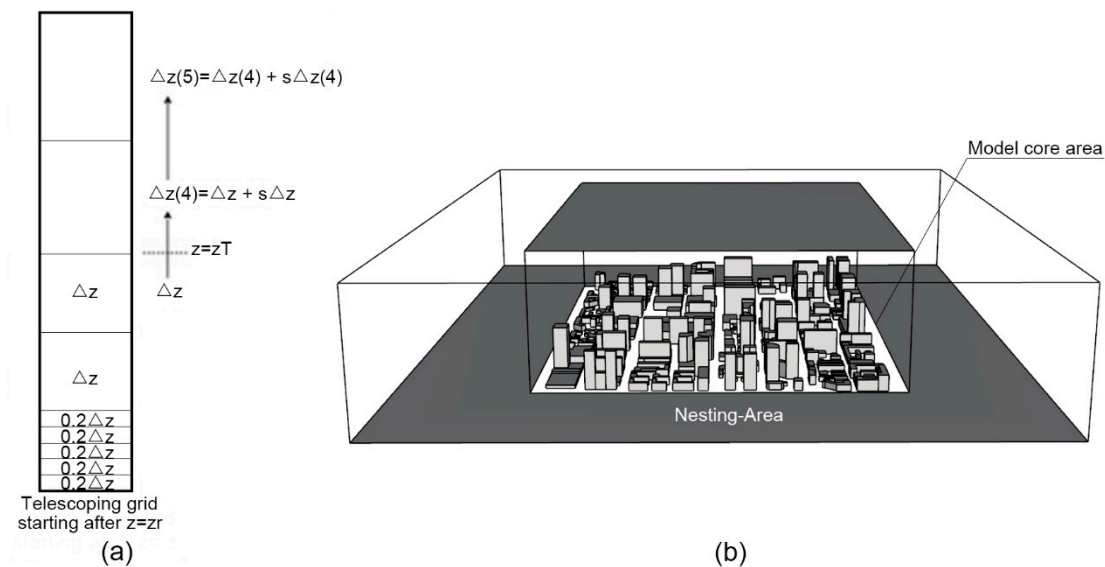

Figure 4. (**a**) Resolution of the vertical grids [43]; (**b**) a schematic diagram of the nesting area.

Field measurements were conducted on 11 April 2019 from 10:00 to 15:00. Three measurement points were selected from the studied district (Figure 5). The hourly air temperatures of the three points at a height of 1.5 m were recorded by handheld digital thermometers (JT Technology, JTR08). The geometric model in Figure 5 was constructed for the evaluation scenario with 70×70 horizontal grids and 30 vertical grids. The horizontal grid resolution was 3 m, and the settings of the nesting area and vertical grids were consistent with those of the experiment scenario.

Figure 5. Location of the measurement points.

2.3.2. Parameter Settings and Model Evaluation

For the evaluation scenario, the initial climate parameters were set according to the data from a meteorological station. The simulation was run from 5:00 to 15:00. The starting air temperature and

relative humidity were 4 °C and 57%, respectively. The wind speed was 2.5 m/s, and the direction was 247.5° (N = 0°, E = 90°) according to the prevailing wind direction during the period of the field measurements. The intensity of the hourly solar radiation was calculated by ENVI-met in accordance with the longitude and latitude of Shenyang.

For the experiment scenario, the meteorological data from 30 July 2018 provided by the meteorological station were selected as the initial climatic parameters. The simulation was run from 4:00 to 18:00. The starting air temperature and relative humidity were 25 °C and 82%, respectively. The direction and speed of the wind were 202.5° and 2.8 m/s, respectively, which were both constant during the whole simulation process. Table 1 presents a summary of all of the input parameters for the simulations of the evaluation and experiment scenario.

Table 1. Summary of input parameters.

Simulation Parameters	Evaluation Scenario	Experiment Scenario
Day	11 April	30 July
Start time	05:00	04:00
Simulation duration	10 h	14 h
Simple forcing: air temperature (°C)	Min 4 at 5:00; max 20.4 at 13:00	Min 25 at 4:00; max 37 at 15:00
Simple forcing: relative humidity (%)	Min 10.7 at 13:00; max 57 at 5:00	Min 52 at 13:00; max 82 at 4:00
Wind direction	247.5°	202.5°
Wind speed at 10 m (m/s)	2.5	2.8
Cloud cover	0	0
Lateral boundary conditions	Simple forcing	Simple forcing
Materials of buildings	Lightweight concrete	Lightweight concrete
Materials of roads	Concrete pavement	Concrete pavement

2.4. Urban Morphological Indicators

Many quantifiable indicators can describe urban morphology. In the scope of this study, 12 urban morphological indicators (Table 2) were selected to investigate their correlation with air temperature. The illustration of enclosure degree (ED) is shown in Figure 6. Each of these indicators met at least one of the following criteria:

- It has a direct effect on the urban thermal environment.
- It impacts the wind field or solar availability and, thus, the process of heat exchange in urban canyons.
- It reflects the heterogeneity of urban morphology.

Table 2. The urban morphological indicators.

| Indicators	Description or Calculation Method
Building footprint ratio (BFR)	BFR = $\sum$(area of building footprint/site area)
Mean building height (MH)	MH = $\sum$(Height of building)/number of buildings (m)
Mean height weighted by footprint area (MHW)	MHW = $\sum$(volume of building)/$\sum$(area of building footprint) (m)
Total height to total floor area ratio (HA)	HA = $\sum$(height of building)/$\sum$(area of building footprint/site area) (m)
Complexity (Cex)	Cex = $\sum$(area of building envelope/site area)
Compactness (Com)	Com = $\sum$(area of building envelope/volume of building) (m^2/m^3)
Mean building volume (MV)	MV = $\sum$(building volume)/number of building (m^3)
Sky view factor (SVF)	A dimensionless parameter representing the ratio of visible sky at a certain location, which is calculated in ENVI-met
Front area ratio (FAR)	FAR = $\sum$(area of vertical wall facing the wind direction)/site area
Enclosure degree (ED)	ED = $\sum$(length of the underside of vertical wall facing the wind direction)/length of edge side of enclosed block (Figure 6)
Standard deviation of building height (SDH)	Describing the vertical heterogeneity of urban morphology (m)
Standard deviation of building footprint area (SDF)	Describing the horizontal heterogeneity of urban morphology (m^2)
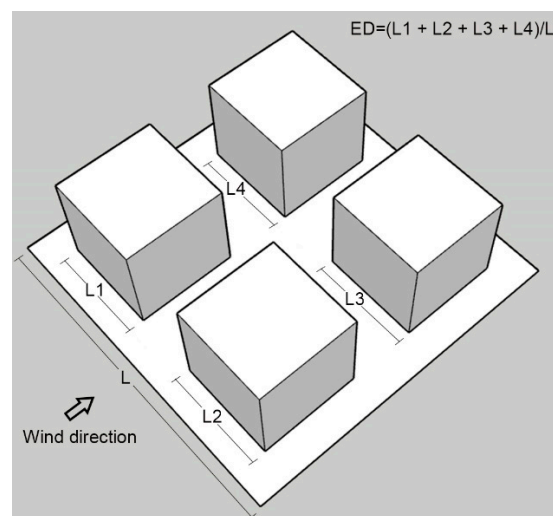
Figure 6. Illustration of the calculation of the enclosure degree (ED).

3. Results

3.1. The Results of the Model Evaluation

The temporal variations of the measured and simulated temperatures at the three points are shown in Figure 7. The variations of the simulated temperatures at point 2 and point 3 showed better consistency with the measured temperature than that at point 1. The differences between the measured and simulated temperatures at point 1 were small at 10:00, 14:00 and 15:00 but relatively evident from 11:00 to 13:00. The differences may be caused by the anthropogenic heat from the surrounding buildings and vehicles, which is more influential in central business districts.
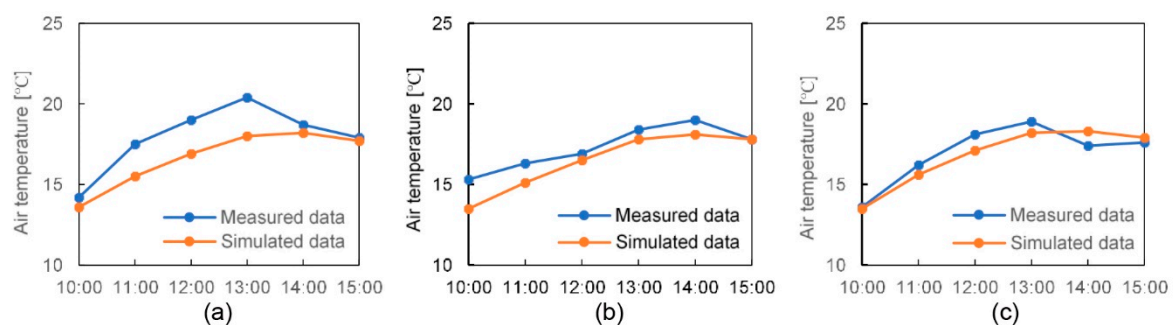

Figure 7. Temporal variation of the measured and simulated temperatures at (**a**) point 1, (**b**) point 2 and (**c**) point 3.

The coefficient of determination (R^2), root mean square error (RMSE) and mean absolute percentage error (MAPE) between the measured and simulated temperatures of the evaluation scenario were calculated to evaluate the reliability of the ENVI-met model. The results of the model evaluation are listed in Table 3. The R^2 ranged from 0.79 to 0.92, the RMSE ranged from 0.68 to 1.57 and the MAPE ranged from 3.42% to 7.00%, which is consistent with a previous study [44].

Table 3. Results of the model evaluation.

Measurement Point	R^2	RMSE	MAPE
1	0.79	1.57	7.00%
2	0.92	1.00	4.92%
3	0.86	0.68	3.42%

3.2. Mesoscale Air Temperature Pattern

In this study, all of the discussed air temperatures refer to the air temperature at the height of 1.5 m above the ground. The distribution of the air temperature and the shadows on the ground at 9:00, 12:00, 14:00 and 17:00 are shown in Figure 8. At each time, the air temperature was classified into three levels, namely, high, medium and low.
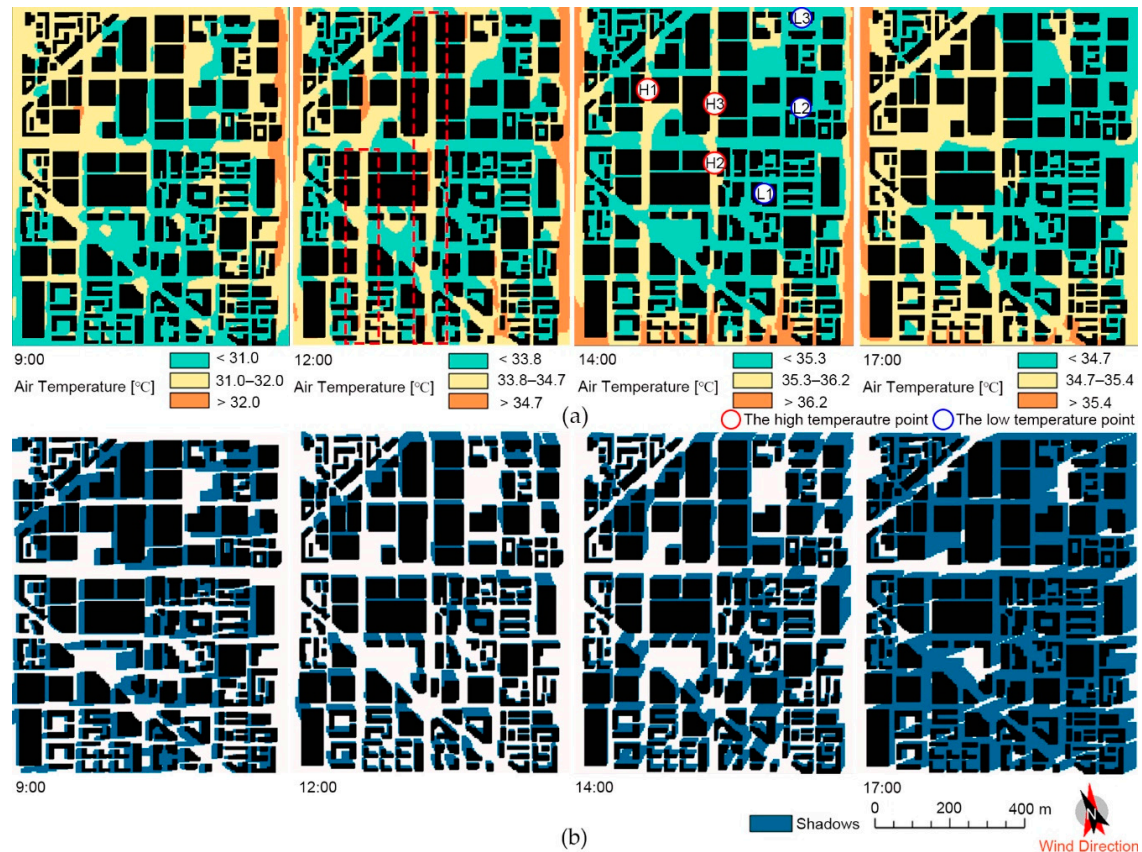

Figure 8. (**a**) The air temperature patterns at 9:00, 12:00, 14:00 and 17:00; (**b**) distribution of the shadows on the ground at 9:00, 12:00, 14:00 and 17:00.

Figure 8 indicates that the location of the high temperature area varied over time due to the change in the solar azimuth and altitude. At 9:00, the air temperatures along the N–S streets were generally lower than those along the E–W streets, mainly because the shadows were on the west side of the buildings in the morning. At 12:00, most of the N–S streets were exposed to direct solar radiation. The shadow area near the buildings reached its minimum due to the largest solar altitude being at 12:00. The air temperatures along the two N–S streets (circled by the dotted line) became evidently higher than those along the other directions, indicating that they were affected the most by the direct solar radiation from 9:00 to 12:00. At 14:00, the shadows turned to the northeast side of the buildings and became larger. At 17:00, most exterior grounds were shadowed by the buildings, except for a few areas exposed to direct solar radiation. The air temperatures in the spaces exposed to solar radiation and between large-footprint buildings were higher.

Three points with the highest air temperatures (H1, H2 and H3) and three points with the lowest temperatures (L1, L2 and L3) at 14:00 were selected to further investigate the thermal environment of the urban district, as shown in Figure 8a. The dynamic variations of the air temperature at these six points from 9:00 to 18:00 are illustrated in Figure 9. At 9:00, the overall temperature difference between the H group and the L group was small. From 12:00 to 15:00, the temperatures of the two groups exhibited relatively obvious differences, and the maximum difference exceeded 2 °C. After 15:00,

the temperature differences between the two groups decreased gradually. This trend indicates that the spatial temperature variation was most obvious in the afternoon, which is valuable to study.
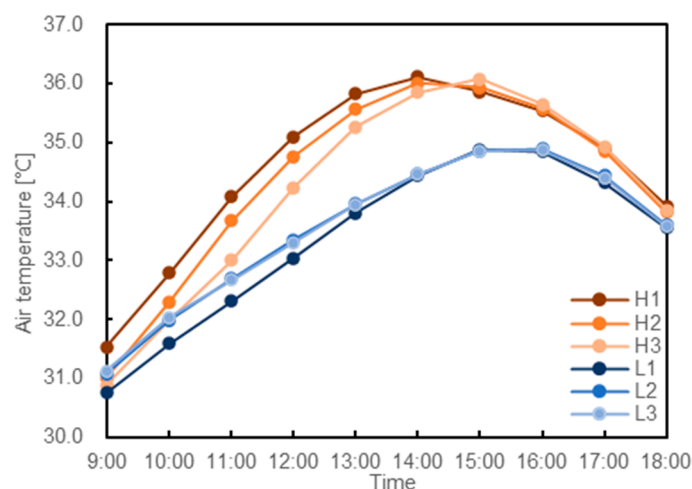

Figure 9. Hourly temperature variation of the H (highest air temperatures) group and L (lowest air temperatures) group.

3.3. Microscale Air Temperature Pattern

Four representative microscale regions of 400×400 m^2 were selected from the studied district, namely, region A (RA), region B (RB), region C (RC) and region D (RD). Their top views and the distribution of the air temperature at 14:00 are shown in Figure 10. Generally, the four regions all contained buildings with different volumes and heights. The urban spaces of RA, RB and RC were relatively more heterogeneous because of the existence of open squares in them. The maximal temperature differences within the four regions were 1.70, 1.49, 1.28 and 1.03 °C, respectively, which were all less than those on the mesoscale.

The hottest areas in RA and RB were both concentrated on the leeward side of the open squares. The hottest areas in RC and RD were both distributed along the N–S streets, and the range of temperature variation in RD was the lowest among the four regions. In all four regions, the areas with the lowest air temperature were located on the north side of the buildings because of their shading and advective effects, which weakened the influence of the hot airflow from the direction of the southwest.

The air temperatures around the same building could also vary a lot. Buildings with the largest surrounding temperature differences in each region are marked by letters (A, B, C and D) in Figure 10. Four evaluation points, one on each side of the building, were selected. The dynamic temperature changes at the evaluation points and the maximum temperature differences around each building are shown in Figure 11. The maximum temperature differences around the four buildings were 1.48, 0.79, 1.19 and 1.12 °C, respectively, all occurring approximately from 13:00 to 14:00. The four buildings were all adjacent to the hottest areas in each region and featured large footprints or high-rises, which provided prominent effects on the shading and advection and led to an evident temperature difference around them.
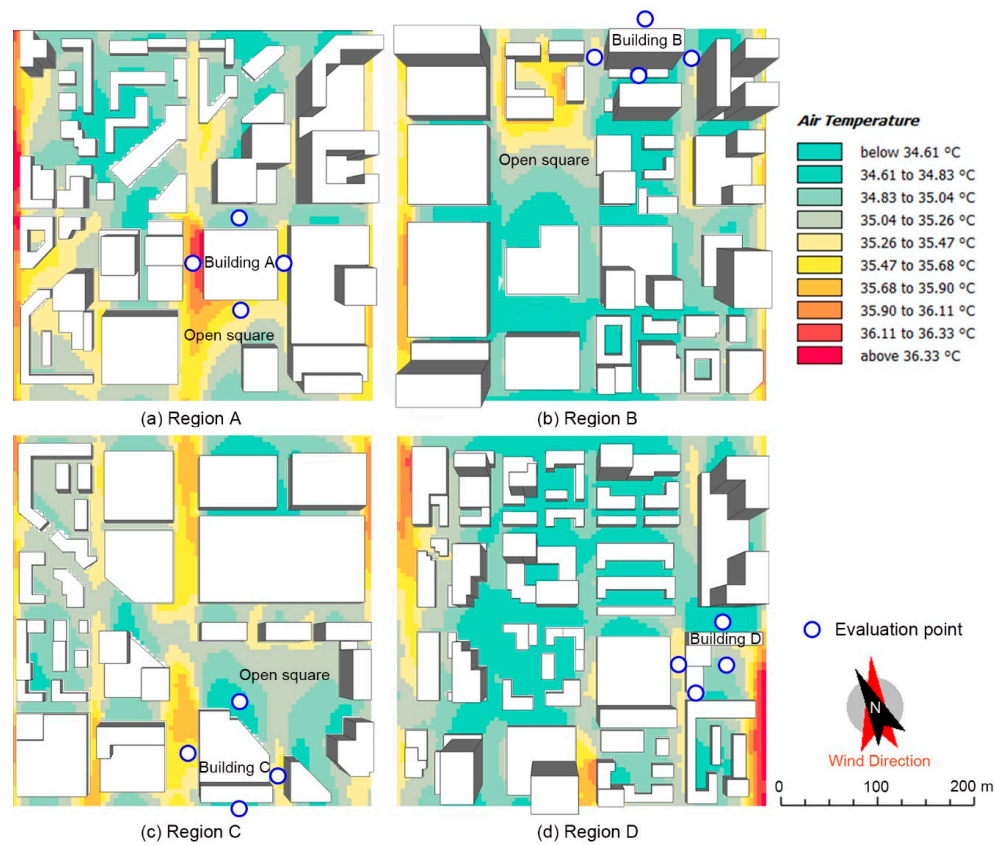
Figure 10. The air temperature patterns in the representative regions: (**a**) in region A, (**b**) in region B, (**c**) in region C and (**d**) in region D.
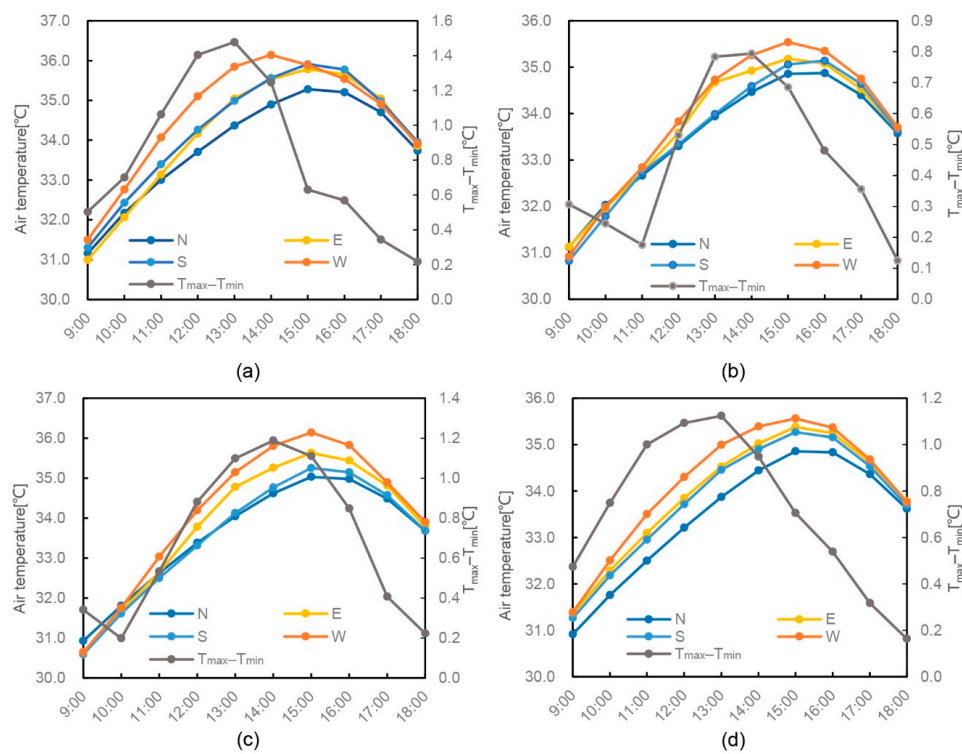

Figure 11. Hourly temperatures at the four sides around a single building and their hourly maximal differences: (**a**) around building A, (**b**) around building B, (**c**) around building C and (**d**) around building D.

3.4. Relationship between Air Temperature and Urban Morphology within the Mesoscale

Sections 3.2 and 3.3 demonstrated that urban morphology had a clear impact on the air temperature pattern both on the mesoscale and the microscale. This section and the next section are intended to establish and quantify the relationship between the air temperature and urban morphology on the mesoscale and the microscale.

3.4.1. Selection of Temperature Representative Points

When simulating the thermal environment with computational fluid dynamics (CFD) software, the air temperatures at the inflow boundary were usually higher than those at the core area because of the unshaded nesting area. This phenomenon may lead to a negative relationship between air temperature and the distance to the inflow boundary. In order to ensure that the temperatures at the representative points were not affected by the inflow, we extracted three temperature profiles at the 67th, 89th and 112th grid on the x-axis along the direction of the inflow (Figure 12a). As illustrated in Figure 12b, the abscissa axis is the distance to the inflow boundary, which is expressed by the grid number on the y-axis in Figure 12a. From the model boundary (grid number = 0) to the 43rd grid, the air temperatures along the three profiles dropped dramatically, and after that, there was no evident relationship between air temperature and grid number.
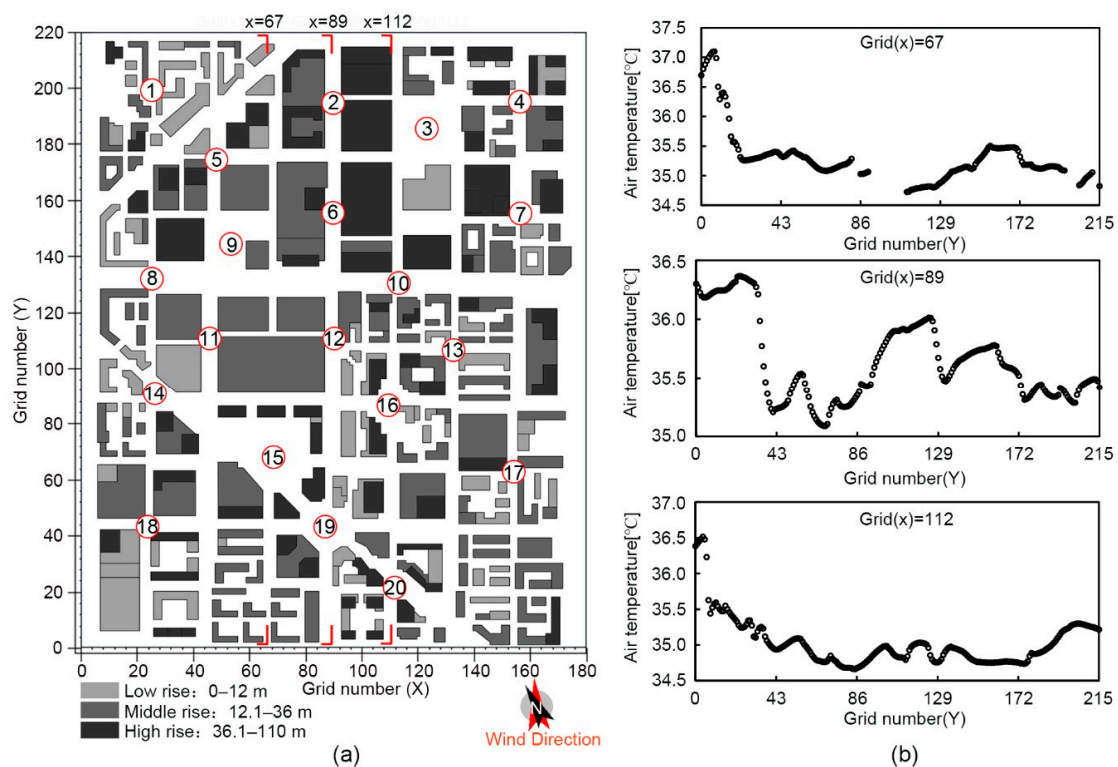

Figure 12. (**a**) Location of the 20 representative points; (**b**) temperature profile along the y-axis at the 67th, 89th and 112th grid on the x-axis.

The correlation between the air temperature after different grid numbers on the y-axis and the distance to the inflow boundary were tested by regression analysis. The determination coefficient (R^2), significance index (sig.) and standardized coefficient (beta) are shown in Table 4. When the value of sig. exceeded 0.05 or beta turned positive, the air temperature could be recognized as independent from the temperature at the inflow boundary. According to this criterion, the temperatures on axes x = 112, x = 89 and x = 67 were not affected by the inflow temperature after the first 20, 25 and 40 grids on the y-axis, respectively.

Table 4. Correlation statistics for the air temperature and the distance to the inflow boundary when discarding different numbers of grids at the beginning of the y-axis.

Coordinate	$y \geq 0$			$y \geq 20$			$y \geq 25$			$y \geq 40$		
	R^2	Sig.	Beta	R^2	Sig.	Beta	R^2	Sig.	Beta	R^2	Sig.	Beta
x = 67	0.277	0.000	−0.526	0.059	0.002	−0.242	0.048	0.006	−0.219	0.013	0.169	−0.116
x = 89	0.176	0.000	−0.420	0.042	0.004	−0.205	0.012	0.131	−0.11	0.026	0.034	0.160
x = 112	0.157	0.000	−0.396	0.000	0.805	−0.018	0.006	0.288	0.077	0.130	0.000	0.360

According to the results above, a total of 20 representative points were selected. The locations of each point are shown in Figure 12a. For points 18, 19 and 20, which were the closest to the inflow boundary, there remained 7 to 22 grids from the region influenced by the inflow temperature. Their air temperatures were largely independent of the direct impact of the inflow.

3.4.2. The Correlation between Urban Morphology Indicators and Air Temperature

The 12 urban morphological indicators, as shown in Table 2, were calculated over a grid 200 m wide centered by each representative point (Figure 3). The correlations between these indicators and the hourly temperatures from 12:00 to 15:00 were tested by curve estimation. The indicators and the air temperatures were fitted to different models, including linear, quadratic, logarithmic, exponential, reciprocal and power models. The coefficients of determination (R^2) and the significance indices (sig.) of the best-fitting model of each indicator are listed in Table 5. A total of six indicators, namely, the building footprint ratio (BFR), total height to total floor area ratio (HA), compactness (Com), mean building volume (MV), enclosure degree (ED) and standard deviation of building footprint area (SDF), were found to be significantly correlated to the air temperature. At 14:00, the significant indices of these indicators were all less than 0.01. The Com showed the strongest effect on the air temperature, with an R^2 value of 0.59. The R^2 of the BFR and ED were both larger than 0.4, and the R^2 of the HA, MV and SDF were relatively lower.

Table 5. Correlation statistics for the morphological indicators and air temperature from 12:00 to 15:00.

Description Variables	12:00		13:00		14:00		15:00	
	R^2	Sig.	R^2	Sig.	R^2	Sig.	R^2	Sig.
BFR	0.27	0.019 *	0.48	0.001 **	0.49	0.003 **	0.33	0.009 **
MH	0.01	0.636	0.00	0.845	0.02	0.846	0.02	0.527
MHW	0.08	0.485	0.01	0.670	0.03	0.483	0.07	0.271
HA	0.23	0.032 *	0.28	0.016 *	0.36	0.006 **	0.40	0.003 **
Cex	0.07	0.265	0.04	0.419	0.07	0.260	0.18	0.064
Com	0.29	0.014 *	0.47	0.001 **	0.59	0.000 **	0.56	0.000 **
MV	0.16	0.084	0.32	0.010 **	0.33	0.009 **	0.22	0.040 *
SVF	0.05	0.363	0.18	0.060	0.16	0.078	0.19	0.161
FAR	0.07	0.259	0.03	0.454	0.06	0.316	0.13	0.114
ED	0.16	0.079	0.35	0.006 **	0.44	0.001 **	0.41	0.002 **
SDH	0.04	0.426	0.02	0.568	0.04	0.407	0.11	0.149
SDF	0.16	0.085	0.30	0.013 *	0.33	0.008 **	0.28	0.017 *

The data with positive and negative correlations are shaded in light and dark grey, respectively. The sig. at 0.05 and 0.01 levels are marked by * and **, respectively.

The other six indicators, namely, the mean building height (MH), mean height weighted by footprint area (MHW), complexity (Cex), sky view factor (SVF), front area ratio (FAR) and standard deviation of building height (SDH), had no significant correlation with the air temperature. With the dramatic variation of the building heights, the MH and MHW were not capable of quantifying the realistic building height level. The SVF showed no significant correlation with the air temperature, possibly because its effect was weakened by other spatial indicators and the advection effects from the wider surroundings of a particular location [21,45]. The FAR, Cex and SDH have been found to be

related to the natural ventilation or the solar access but showed no correlation with the air temperature, either [30,46].

3.4.3. The Effect of the Urban Morphology Indicators

Figure 13 illustrates the linear and best-fit models for the correlation between the six significant indicators and the air temperatures at the 20 representative points, namely point 1 to point 20 (P1 to P20). Figure 13a indicates a generally positive correlation between the BFR and the air temperature. The BFR represents the density of buildings. The increase in the BFR can lead to more reflected radiation and less heat dissipation by longwave radiation inside the street canyon [47] and, thus, causes the air temperature to rise. Figure 13b indicates a negative correlation between the ED and the air temperature. The ED may influence the air temperature by affecting the wind speed and heat convection. The increase in the ED can reduce the effect of hot ambient temperatures in the summertime. Figure 13c indicates a negative correlation between the HA and the air temperature. The increase in the HA means a decrease in building density or an increase in building height, which enhances the cooling effect. Figure 13d indicates that the Com was negatively correlated to the air temperature. According to Figure 14, the Com was significantly correlated with the BFR and ED, while the correlation between the BFR and ED was relatively weak. This indicates that in the studied district, the Com was correlated with two influential morphological features for air temperature, which may have contributed to a greater R^2 for the Com.
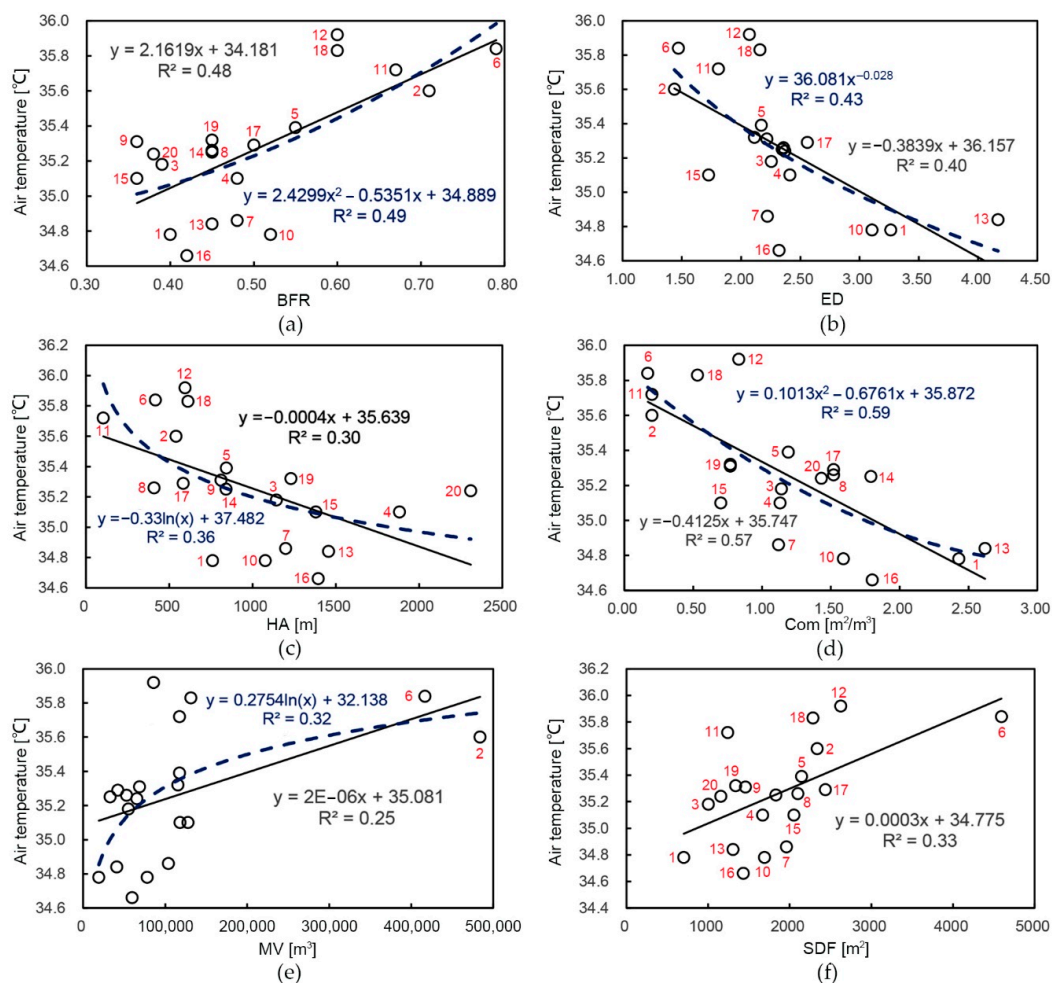

Figure 13. Correlation between morphological indicators and air temperature at 14:00: (**a**) BFR and air temperature, (**b**) ED and air temperature, (**c**) HA and air temperature, (**d**) Com and air temperature, (**e**) MV and air temperature and (**f**) SDF and air temperature.
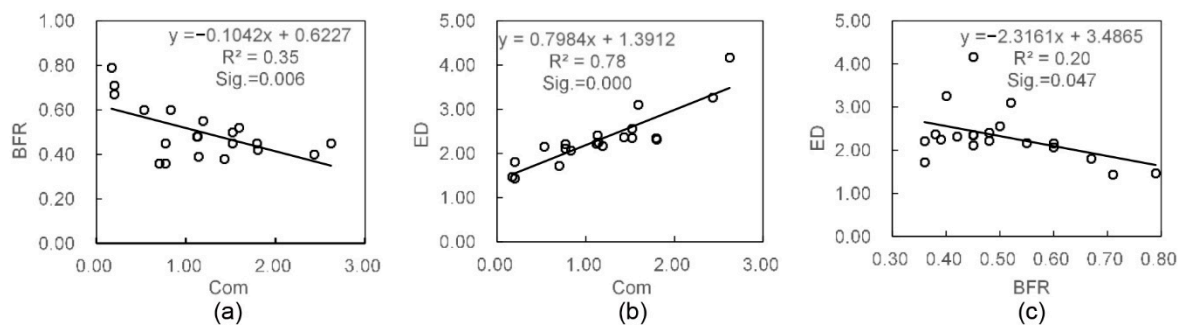
Figure 14. Relationship between (**a**) Com and BFR, (**b**) Com and ED and (**c**) BFR and ED.

Although Figure 13e indicates a positive correlation between the MV and the air temperature, the coefficient of determination was only 0.33. The data from P2 and P6 had an important influence on the results of the curve estimation. Discarding the two points, the correlation between the MV and air temperature failed to reach the significance level ($R^2 = 0.19$, sig. $= 0.069$). The SDF had a positive correlation with the air temperature according to Figure 13f, which may not have been caused by the horizontal heterogeneity of urban morphology. For example, the SDF of P6 was the largest, but its surrounding horizontal building arrangement was homogeneous. The high temperature of P6 was caused by the high density and lack of shadows.

3.5. Relationship between Air Temperature and Urban Morphology on the Microscale

3.5.1. The Correlation between Urban Morphology Indicators and Air Temperature

We selected 12 representative points from each microscale region in Figure 10, and the locations of the points are shown in Figure 15. The morphological indicators that were proved to be significant in the mesoscale analysis, including the BFR, HA, Com and ED, together with the MH, were calculated over a grid 100 m wide centered by each representative point (Figure 3).

The correlations between the indicators and the air temperature at 14:00 within each region were tested by curve estimation. The R^2 and sig. of the best-fitting models of each indicator are shown in Table 6. The correlations between the indicators and the air temperature were different among the four regions. The BFR and ED were most frequently correlated to the air temperature and were significant indicators in RA, RC and RD. The R^2 of the ED ranged from 0.44 to 0.73 in the three regions, while the R^2 of the BFR ranged from 0.43 to 0.49, indicating the ED to be more influential than the BFR for the air temperature on the microscale.

Table 6. Correlation statistics for the morphological indicators and the air temperature at 14:00 in region A, region B, region C and region D.

Description Variables	Region A		Region B		Region C		Region D	
	R^2	Sig.	R^2	Sig.	R^2	Sig.	R^2	Sig.
BFR	0.49	0.050 *	0.13	0.253	0.43	0.021 *	0.49	0.011 *
MH	0.11	0.220	0.16	0.463	0.26	0.219	0.24	0.289
HA	0.16	0.225	0.15	0.366	0.45	0.017 *	0.03	0.586
Com	0.57	0.007 **	0.09	0.646	0.21	0.138	0.55	0.029 *
ED	0.73	0.000 **	0.17	0.182	0.55	0.006 **	0.44	0.019 *

The data with positive and negative correlations are shaded in light and dark grey, respectively. The sig. at 0.05 and 0.01 levels are marked by * and **, respectively.

However, the Com and HA were less influential compared with the BFR and ED. The Com was tested to be a significant indicator in RA and RD, and the HA only affected the air temperature in RC. The MH showed no correlation with the air temperature. The correlation between the morphological

indicators and the air temperature was the weakest in RB, and the significance indices of all the indicators exceeded 0.05.
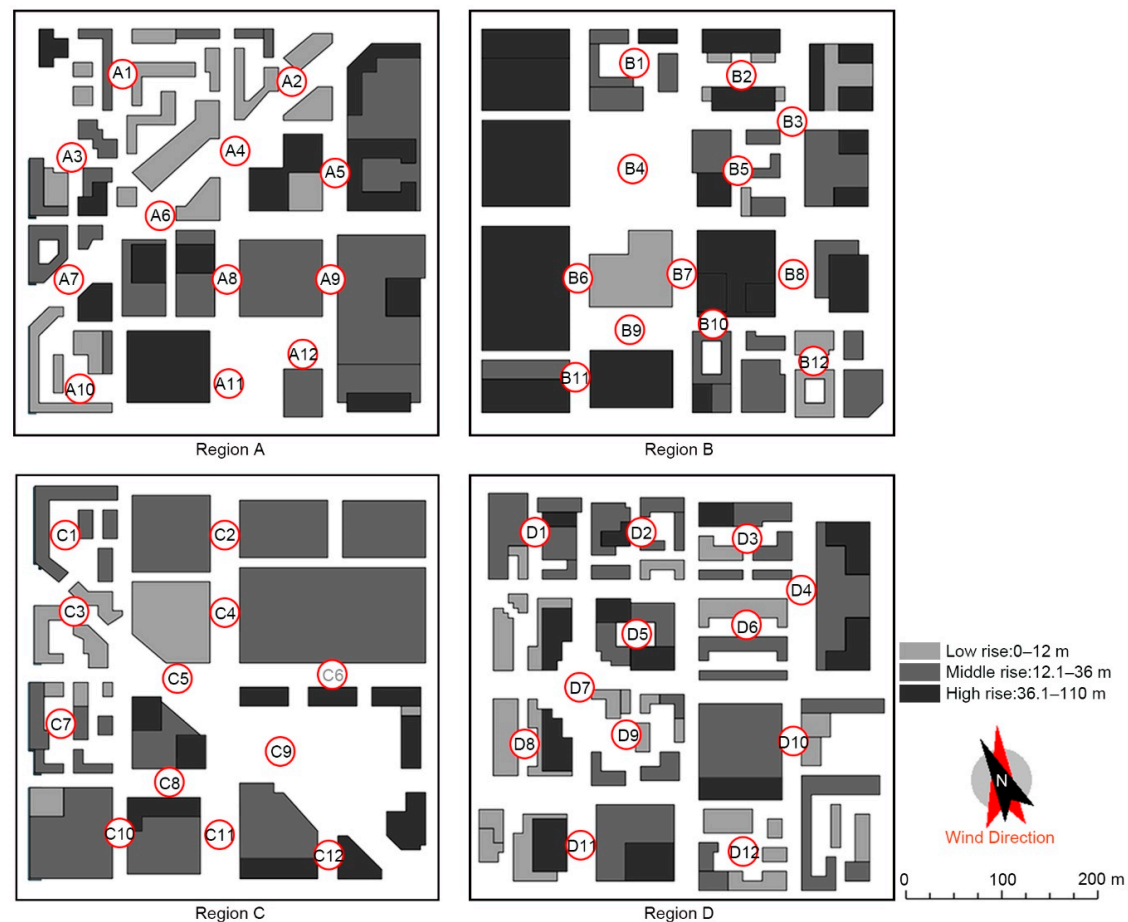

Figure 15. Locations of the representative points in region A, region B, region C and region D.

3.5.2. The Effect of the Urban Morphology Indicators

Figure 16 illustrates the regression curve for the correlation between the BFR, ED and the air temperature at the 12 representative points in each region. In region A, the quadratic model for the BFR and the air temperature fit the best. When the BFR was lower than 0.5, it showed a negative relationship with the air temperature. After the BFR exceeded 0.5, the relationship became positive. The ED had a strong correlation with the air temperature, with an R^2 of 0.73 (Figure 16a). In region B, the BFR and ED both showed poor correlations with the air temperature, although the general trends of their regression curves were negative (Figure 16b). In region C and region D, the air temperature was positively correlated to the BFR and negatively correlated to the ED (Figure 16c,d).

The correlation between the BFR and the air temperature in RA was different from that in RC and RD. According to Figures 15 and 16, the points in low-density plots (such as A11 and A4) in RA were not blocked by buildings in the windward direction. Meanwhile, most of the points in low-density plots (such as C9 and D9) in RC and RD were at the leeward side of buildings, which weakened the influence of the inflow temperature. As illustrated in Figure 16, the ED values of C9 and D9 were larger than that of A11, which proved this inference.

The poor statistical correlation between morphological indicators and the air temperature in RB can be explained by the distinct microclimate around the open square. Figure 16b indicates that the point B1 deviated significantly from the regression curve of the BFR and ED. According to Figures 10b and 15, B1 was located on the leeward side of the open square, which suffered excessive solar radiation.

The temperature within the open square increased gradually along the wind direction and led to an obviously higher ambient temperature for B1 compared with that of other points.
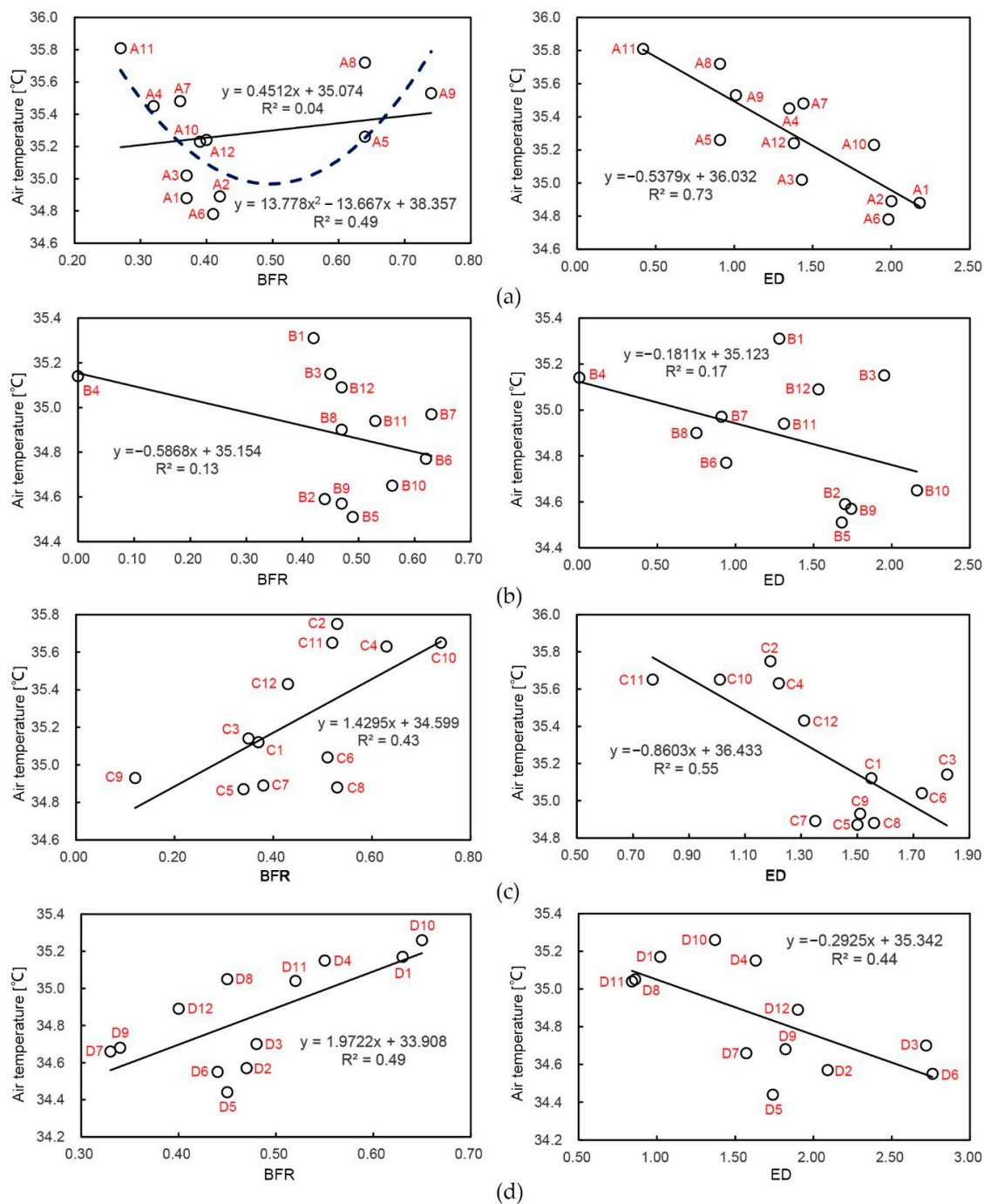

Figure 16. Correlation between air temperature and BFR and ED in (**a**) region A, (**b**) region B, (**c**) region C and (**d**) region D.

4. Discussion

4.1. The Correlation between Urban Morphology and Air Temperature on Different Scales

On the mesoscale, the BFR, HA, Com and ED were found to have significant correlations with the air temperature in the afternoon. Meanwhile, on the microscale, the correlation between morphological indicators and air temperature varied among different regions, and only the BFR and ED were most

frequently correlated to the air temperature. The explanatory power of the same indicator also varied on different scales. On the mesoscale, the Com and BFR showed the strongest correlation with the air temperature, with maximal R^2 values of 0.59 and 0.49, respectively. Meanwhile, on the microscale, the ED turned out to be more influential than the BFR in RA and RC. The R^2 value of the ED ranged from 0.17 to 0.73, while the R^2 value of the BFR ranged from 0.13 to 0.49 among the four regions.

The differences in the correlation between urban morphology and air temperature on different scales can be explained by the following reasons. Firstly, although the BFR and HA can be correlated to air temperature by influencing the temperature of the underlying surface, sufficient distance is needed for the temperature upwind to be fully adjusted to the temperature of the underlying surface [17]. Meanwhile, the distances between each representative point on the microscale were not sufficient for the heat exchange between the air temperature and underlying surface, which weakened the effect of these indicators. The advection effect on the microscale influenced by the ED turned out to be more influential to air temperature compared with that on the mesoscale.

Secondly, because the ED mainly influences the heat convection among the plot units, its effect on the air temperature depends on the inflow temperature of the plots. The range of temperature variation on the microscale was smaller than that on the mesoscale, which reduced the difference in the inflow temperature among the plots on the microscale and intensified the correlation between air temperature and the ED. Meanwhile, the air temperatures of plots with similar ED values still varied a lot on the mesoscale because of the relatively wider range of the ambient temperatures (Figure 13b). According to another study in Xi'an, China, the measurement points were selected from a much wider urban area. As a result, the ED was also found to have a negative effect on the air temperature, but the correlation was weaker than that of this study [23].

4.2. The Effect of Heterogeneity on the Correlation between Urban Morphology and Air Temperature

The correlation between urban morphology and the air temperature has been investigated in the literature, and the main conclusions are summarized as follows:

(a)   The BFR has a positive correlation with the air temperature of UHI intensity, and it is the most influential among all of the urban geometric indicators [21–23].

(b)   The HA is negatively correlated to the air temperature [24], and taller buildings lead to lower temperatures due to the shading effect at the street level at 13:00 [48].

(c)   The SVF was found to have a correlation with air temperature in some intensely developed and high-density areas [24], but its thermal effect may be weakened by the advection effects from the wider surrounding areas [21].

(d)   The Cex and SDH were found to affect the solar access and natural ventilation in urban canyons, and the MV only affects natural ventilation [29,30].

In this study, the effects of the BFR, HA and ED on the air temperature found on the mesoscale were consistent with those of previous studies [21–24], although the correlations between air temperature and these indicators on the microscale were weak in some conditions. However, we did not find significant correlations between air temperature and the SVF, MH and Cex, and the Com was found to have a strong effect on the air temperature, all of which was different from previous studies. The poor relation between air temperature and the SVF has been discussed previously, namely, that it is weakened by other spatial indicators and the advection effects from the wider surroundings of a particular location [21,45]. Meanwhile, the other different findings can be explained by the heterogeneous features of the studied district.

Firstly, the building heights and the building footprints in the studied urban district varied dramatically. The same values of the MH, Cex and FAR could be related to building clusters with different morphological features, which led to a distinct thermal performance and weakened the correlation between the air temperature and these indicators. Meanwhile, as illustrated in Figure 14, the buildings with large volumes and low Com constituted plots with high BFRs and low EDs in the

studied district, which led to higher temperatures. In this specific situation, the Com was closely related to two influential morphological features for the air temperature, so it showed the strongest effect on the air temperature in this study.

Secondly, the urban district also exhibited strong horizontal heterogeneity on the plane, which weakened the correlation between air temperature and urban morphology, especially on the microscale. In region B, the open square led to higher ambient temperatures for its leeward side points, such as B1 (Figures 10b and 15). Therefore, the temperature of B1 could be much higher than that of the points with similar morphological indicators, which led to a significant deviation of B1 from the regression curve and weakened the statistical correlation (Figure 16b).

4.3. Urban Morphology Design Strategy for Improving the Urban Thermal Environment

It has been recommended by some studies that optimizing urban morphology on the scale with a radius of several hundred meters can effectively improve pedestrian thermal comfort [22,49]. Indicators including building density, building height, green space ratios and green cover ratios have been found to be influential to the air temperature or UHIs [23,48].

In this study, the BFR, ED, HA and Com were found to have significant effects on the daytime air temperature in a central business district in northeastern China. The decrease in building density or increase in building height could lead to lower air temperatures during the daytime (Figure 13a,c). Although increasing the ED could generally decrease the air temperature, its specific effect also depended on the ambient environment (Figure 13b). When the building clusters were close to cooling spaces such as urban parks and rivers, decreasing the ED could facilitate the cooling effect of the airflow from these spaces. It is also notable that the increase in the Com could lead to lower air temperatures in the studied district. It is because the increase in Com means reducing the building volumes, which is beneficial for decreasing the BFR and increasing the ED (Figure 14). This phenomenon can be more remarkable in central business districts, where the variations of building volumes are usually dramatic.

On the microscale, the ED turned out to be most influential to the air temperature. This indicates that optimizing the building configuration to achieve a proper ED according to the surrounding environment can be the most efficient strategy for improving the thermal environment for plots with side lengths of less than 100 m. Building clusters should be enclosed from the surrounding heating spaces and opened to the cooling spaces. Narrow spaces between buildings should also be avoided for the heat dissipation in street canyons.

5. Conclusions

To investigate the relationship between spatial temperature variation and urban morphology in a heterogeneous city district, a numerical simulation on the summer thermal environment of a central business district in Shenyang was conducted. It was found that the temperature distribution changed with the time because of the variation of the solar azimuth. At 14:00, the air temperatures differed by 2.12 °C in the studied district, while the temperature differences ranged from 1.03 to 1.70 °C within the regions on the microscale.

The results of the curve estimation indicate that the BFR, Com, ED and HA were significantly correlated to the air temperature on the mesoscale. The Com and BFR were the most influential morphological indicators, explaining 59% and 49% of the temperature variation, respectively. The explanatory powers of the ED and HA were relatively weaker, explaining 44% and 40% of the temperature variation, respectively. On the microscale, only the ED and BFR had relatively steady correlations with the air temperature, and the ED was more influential on the microscale than the BFR. The distinctions in the correlation between urban morphology and air temperature on two scales were caused by the different ranges of spatial temperature variation and different distances for heat exchange between the upwind and underlying surfaces.

The heterogeneity indicators SDH and SDF were both not influential indicators in this study, while heterogeneity did affect the correlation between the air temperature and some morphological

indicators. The dramatic distinction in heights and footprints of the buildings weakened the effects of the MH, FAR and Cex on the air temperature. The heterogeneity of the horizontal building layout could enlarge the distinction in the inflow temperature of each plot unit and weaken the statistical correlation between urban morphology and air temperature.

The results of this study can help to get a deeper understanding about the correlation between urban morphology and the air temperature in a heterogeneous urban district. However, the current study may be limited by the fixed wind conditions of the model simulation and limited scale of the studied district. The setting of the nesting area could not consider the impact of the buildings around the model domain. The effect of urban morphology on nocturnal air temperature was not analyzed because of the relatively short simulation period, and the effect of urban green infrastructure was excluded. In the future, measurements will be conducted in the wider urban area to further investigate the effect of urban morphology on the air temperature across different scales. Meanwhile, morphological indicators correlated to the thermal properties of heterogeneous urban districts are supposed to be proposed in the next stage. The thermal performance of a vegetation scenario will be compared with that of a vegetation-free scenario in a future study.

References

1. United Nations. *World Urbanization Prospects: The 2018 Revision*; UN DESA: New York, NY, USA, 2018. [CrossRef]
2. Oke, T.R. *Boundary Layer Climate*, 2nd ed.; Methuen: London, UK, 1987. [CrossRef]
3. Matzarakis, A.; Amelung, B. Physiological equivalent temperature as indicator for impacts of climate change on thermal comfort of humans. In *Seasonal Forecasts, Climatic Change and Human Health*; Thomson, M.C., Garcia-Herrera, R., Beniston, M., Eds.; Springer: Dordrecht, The Netherlands, 2008; Volume 30, pp. 161–172. [CrossRef]
4. Sarrat, C.; Lemonsu, A.; Masson, V.; Guedalia, D. Impact of urban heat island on regional atmospheric pollution. *Atmos. Environ.* **2006**, *40*, 1743–1758. [CrossRef]
5. Santamouris, M. On the energy impact of urban heat island and global warming on buildings. *Energy Build.* **2014**, *82*, 100–113. [CrossRef]
6. Hajat, S.; Vardoulakis, S.; Heaviside, C.; Eggen, B. Climate change effects on human health: Projections of temperature-related mortality for the UK during the 2020s, 2050s and 2080s. *J. Epidemiol. Commun. Health* **2014**, *68*, 641–648. [CrossRef]
7. Erell, E.; Pearlmutter, D.; Williamson, T. *Urban Microclimate: Designing the Spaces between Buildings*, 1st ed.; Earthscan: London, UK; Washington, DC, USA, 2010.
8. Golany, G.S. Urban design morphology and thermal performance. *Atmos. Environ.* **1996**, *30*, 455–465. [CrossRef]
9. Mirzaei, P.A.; Haghighat, F. Approaches to study Urban Heat Island—Abilities and limitations. *Build. Environ.* **2010**, *45*, 2192–2201. [CrossRef]
10. Sassen, S. Bridging the Ecologies of Cities and of Nature. In Proceedings of the 4th International Conference of the International Forum on Urbanism, Amsterdam/Delft, The Netherlands, 26–28 November 2009.
11. Ratti, C.; Raydan, D.; Steemers, K. Building form and environmental performance: Archetypes, analysis and an arid climate. *Energy Build.* **2003**, *35*, 49–59. [CrossRef]
12. Moudon, A.V. Urban morphology as an emerging interdisciplinary field. *Urban Morphol.* **1997**, *1*, 3–10.
13. Chen, X.L.; Zhao, H.M.; Li, P.X.; Yin, Z.Y. Remote sensing image-based analysis of the relationship between urban heat island and land use/cover changes. *Remote Sens. Environ.* **2006**, *104*, 133–146. [CrossRef]

14. Lee, L.; Chen, L.; Wang, X.; Zhao, J. Use of Landsat TM/ETM+ data to analyze urban heat island and its relationship with land use/cover change. In Proceedings of the International Conference on Remote Sensing, Nanjing, China, 24–26 June 2011. [CrossRef]

15. Mohan, M.; Kikegawa, Y.; Gurjar, B.R.; Bhati, S.; Kolli, N.R. Assessment of urban heat island effect for different land use-land cover from micrometeorological measurements and remote sensing data for megacity Delhi. *Theor. Appl. Climatol.* **2013**, *112*, 647–658. [CrossRef]

16. Li, J.; Song, C.; Cao, L.; Zhu, F.; Meng, X.; Wu, J. Impacts of landscape structure on surface urban heat islands: A case study of Shanghai, China. *Remote Sens. Environ.* **2011**, *115*, 3249–3263. [CrossRef]

17. Stewart, I.D.; Oke, T.R. Local climate zones for urban temperature studies. *Bull. Am. Meteorol. Soc.* **2012**, *93*, 1879–1900. [CrossRef]

18. Xu, D.; Zhou, D.; Wang, Y.; Meng, X.; Chen, W.; Yang, Y. Temporal and spatial variations of urban climate and derivation of an urban climate map for Xi'an, China. *Sustain. Cities Soc.* **2020**, *52*, 1–17. [CrossRef]

19. Lee, D.; Oh, K. Classifying urban climate zones (UCZs) based on statistical analyses. *Urban Clim.* **2018**, *24*, 503–516. [CrossRef]

20. Ren, C.; Ng, E.Y.Y.; Katzschner, L. Urban climatic map studies: A review. *Int. J. Climatol.* **2011**, *31*, 2213–2233. [CrossRef]

21. van Hove, L.W.A.; Jacobs, C.M.J.; Heusinkveld, B.G.; Elbers, J.A.; Van Driel, B.L.; Holtslag, A.A.M. Temporal and spatial variability of urban heat island and thermal comfort within the Rotterdam agglomeration. *Build. Environ.* **2015**, *83*, 91–103. [CrossRef]

22. Lan, Y.; Zhan, Q. How do urban buildings impact summer air temperature? The effects of building configurations in space and time. *Build. Environ.* **2017**, *125*, 88–98. [CrossRef]

23. Xu, D.; Zhou, D.; Wang, Y.; Xu, W.; Yang, Y. Field measurement study on the impacts of urban spatial indicators on urban climate in a Chinese basin and static-wind city. *Build. Environ.* **2019**, *147*, 482–494. [CrossRef]

24. Giridharan, R.; Lau, S.S.Y.; Ganesan, S.; Givoni, B. Urban design factors influencing heat island intensity in high-rise high-density environments of Hong Kong. *Build. Environ.* **2007**, *42*, 3669–3684. [CrossRef]

25. Tong, S.; Wong, N.H.; Jusuf, S.K.; Tan, C.L.; Wong, H.F.; Ignatius, M.; Tan, E. Study on correlation between air temperature and urban morphology parameters in built environment in northern China. *Build. Environ.* **2018**, *127*, 239–249. [CrossRef]

26. Yang, F.; Lau, S.S.Y.; Qian, F. Summertime heat island intensities in three high-rise housing quarters in inner-city Shanghai China: Building layout, density and greenery. *Build. Environ.* **2010**, *45*, 115–134. [CrossRef]

27. Grimmond, C.S.B.; Oke, T.R. Aerodynamic properties of urban areas derived from analysis of surface form. *J. Appl. Meteorol.* **1999**, *38*, 1262–1292. [CrossRef]

28. Macdonald, R.W.; Griffiths, R.F.; Hall, D.J. An improved method for the estimation of surface roughness of obstacle arrays. *Atmos. Environ.* **1998**, *32*, 1857–1864. [CrossRef]

29. Edussuriya, P.; Chan, A.; Ye, A. Urban morphology and air quality in dense residential environments in Hong Kong. Part I: District-level analysis. *Atmos. Environ.* **2011**, *45*, 4789–4803. [CrossRef]

30. Chatzipoulka, C.; Compagnon, R.; Nikolopoulou, M. Urban geometry and solar availability on façades and ground of real urban forms: Using London as a case study. *Sol. Energy* **2016**, *138*, 53–66. [CrossRef]

31. Oke, T.R. Initial guidance to obtain representative meteorological observations at urban sites. In *World Meteorological Organization No. 1250, Instruments and Observing Methods Report No. 81*; WMO: Geneva, Switzerland, 2006.

32. Pacifici, M.; Rama, F.; de Castro Marins, K.R. Analysis of temperature variability within outdoor urban spaces at multiple scales. *Urban Clim.* **2019**, *27*, 90–104. [CrossRef]

33. Middel, A.; Häb, K.; Brazel, A.J.; Martin, C.A.; Guhathakurta, S. Impact of urban form and design on mid-afternoon microclimate in Phoenix Local Climate Zones. *Landsc. Urban Plan.* **2014**, *122*, 16–28. [CrossRef]

34. Allegrini, J.; Dorer, V.; Carmeliet, J. Influence of morphologies on the microclimate in urban neighbourhoods. *J. Wind Eng. Ind. Aerodyn.* **2015**, *144*, 108–117. [CrossRef]

35. Taleghani, M.; Kleerekoper, L.; Tenpierik, M.; Van Den Dobbelsteen, A. Outdoor thermal comfort within five different urban forms in the Netherlands. *Build. Environ.* **2015**, *83*, 65–78. [CrossRef]

36. Chatzidimitriou, A.; Yannas, S. Street canyon design and improvement potential for urban open spaces; the influence of canyon aspect ratio and orientation on microclimate and outdoor comfort. *Sustain. Cities Soc.* **2017**, *33*, 85–101. [CrossRef]

37. Drach, P.; Krüger, E.L.; Emmanuel, R. Effects of atmospheric stability and urban morphology on daytime intra-urban temperature variability for Glasgow, UK. *Sci. Total Environ.* **2018**, *627*, 782–791. [CrossRef]

38. Krüger, E.; Drach, P.; Broede, P. Outdoor comfort study in Rio de Janeiro: Site-related context effects on reported thermal sensation. *Int. J. Biometeorol.* **2017**, *61*, 463–475. [CrossRef] [PubMed]

39. Sharmin, T.; Steemers, K.; Matzarakis, A. Microclimatic modelling in assessing the impact of urban geometry on urban thermal environment. *Sustain. Cities Soc.* **2017**, *34*, 293–308. [CrossRef]

40. Shenyang Weather Forecast and Shenyang Climate. Available online: http://www.weatherchina.org/shenyang.htm/ (accessed on 3 June 2020).

41. Houet, T.; Pigeon, G. Mapping urban climate zones and quantifying climate behaviors—An application on Toulouse urban area (France). *Environ. Pollut.* **2011**, *159*, 2180–2192. [CrossRef] [PubMed]

42. ENVI-met Model Architecture. Available online: http://envi-met.info/doku.php?id=intro:modelconcept./ (accessed on 3 June 2020).

43. Vertical Grid Layout. Available online: http://envi-met.info/doku.php?id=kb:verticalgrid&s[]=telescoping/ (accessed on 3 June 2020).

44. Morakinyo, T.E.; Lau, K.K.L.; Ren, C.; Ng, E. Performance of Hong Kong's common trees species for outdoor temperature regulation, thermal comfort and energy saving. *Build. Environ.* **2018**, *137*, 157–170. [CrossRef]

45. Blankenstein, S.; Kuttler, W. Impact of street geometry on downward longwave radiation and air temperature in an urban environment. *Meteorol. Z.* **2004**, *13*, 373–379. [CrossRef]

46. Ng, E.; Yuan, C.; Chen, L.; Ren, C.; Fung, J.C.H. Improving the wind environment in high-density cities by understanding urban morphology and surface roughness: A study in Hong Kong. *Landsc. Urban Plan.* **2011**, *101*, 59–74. [CrossRef] [PubMed]

47. Lin, P.; Gou, Z.; Lau, S.S.Y.; Qin, H. The impact of urban design descriptors on outdoor thermal environment: A literature review. *Energies* **2017**, *10*, 2151. [CrossRef]

48. Perini, K.; Magliocco, A. Effects of vegetation, urban density, building height, and atmospheric conditions on local temperatures and thermal comfort. *Urban For. Urban Green.* **2014**, *13*, 495–506. [CrossRef]

49. Wang, Z.H.; Fan, C.; Myint, S.W.; Wang, C. Size Matters: What are the characteristic source areas for urban planning strategies? *PLoS ONE* **2016**, *11*, e0165726. [CrossRef]